17th World Conference on Earthquake Engineering, 17WCEE
Sendai, Japan - September 13th to 18th 2020

DEVELOPMENT OF A THERMOMECHANICAL HYBRID TESTING PLATFORM FOR FIRE FOLLOWING EARTHQUAKE SIMULATIONS

A. Sauca[(1)], N. Mortensen[(2)], A. Drustrup[(3)], G. Abbiati[(4)]

[(1)] *Post.doc Scientific Researcher, DBI – The Danish Institute of Fire and Security Technology, as@dbigroup.dk*
[(2)] *Research Consultant, DBI – The Danish Institute of Fire and Security Technology, nmo@dbigroup.dk*
[(3)] *Resistance to Fire Engineer, DBI – The Danish Institute of Fire and Security Technology, adr@dbigroup.dk*
[(4)] *Assistant Professor, Department of Engineering, University of Aarhus, abbiati@eng.au.dk*

Abstract

Fires following earthquakes have produced historically large post-earthquake damage. The failure of non-structural components has an impact on the building fire performance, e.g. egress delay from the building, faster spread of fire, quicker temperature rise in the structural elements due to damage in the fire protection system. Thus, the vulnerability to the fire following earthquake of the structural system, which has been already weakened by the seismic event, can greatly increase. In a performance-based approach, it would be sensible to evaluate the effect of an earthquake on the fire safety level for buildings located in seismic-prone zones even if there are no standards currently addressing this issue. This paper presents the hybrid testing platform developed at the Danish Institute of Fire and Security Technology to investigate the structural performance and fire resistance following earthquakes of gypsum plasterboards based walls. Experimental errors and thermo-mechanical properties of gypsum plasterboards at elevated temperatures are characterized to support the numerical verification of the proposed hybrid fire testing framework reported in this paper.

Keywords: fires following earthquakes, hybrid testing, fire resistance, gypsum plasterboard.

1 Introduction

Fire following earthquake (FFE) has produced historically massive post-earthquake damage. For instance, fires following the San Francisco 1906 earthquake caused significant property losses: 28000 buildings were destroyed for a value of approximately 250 M$ in 1906 dollars and 3000 life losses [1]. The post-earthquake fire caused by the 1923 Tokyo earthquakes lasted 3 days and caused 77% of the damage [2]. These two earthquakes are the cause of the two largest urban fires, where the damage caused by the fire was higher than the damage due to the ground shaking. Also, the 1995 Kobe earthquake triggered 140 fires and the water supply was available only for 2 to 3 hours [3]. The 1999 Turkey earthquake and 2011 Tohoku earthquake caused major fires in oil & refineries that lasted several days. In the 2011 Christchurch earthquake, many secondary structural components as staircases and non-structural components such as façade systems, ceilings, interior walls, fireproofing systems, etc. were severely damaged. It is clear that failure of non-structural components has an impact on the building fire performance i) egress delay from the building; ii) faster spread of fire; iii) quicker temperature rise in the structural elements due to damage in the fire protection system [4]. Thus, the vulnerability to FFE of the structural system, which has been already weakened by the seismic event, can significantly increase. In a performance-based approach, it would be sensible to evaluate the effect of an earthquake on the fire safety level for buildings located in seismic-prone zones. However, no standards currently address this issue and the two actions are accounted for separately. In this context, it is legitimate to foresee that if FFE will continue to be inadequately addressed, this can lead to major disasters again. Few attempts have been carried out to experimentally investigate the effect of an earthquake on the fire performance of structural and non-structural components. In particular, Pucinotti and co-workers [5], [6] analyzed the post-earthquake fire behavior of beam-to-concrete filled steel tube column joints. The low-cycle fatigue tests were performed at the lab facility of the University of Trento whereas the fire tests followed at the Building Research Establishment (BRE) in the UK. Since it was not practical to deliver the seismically-damaged specimens to the UK, at the BRE some specimens were pre-damaged before being subjected to fire loadings by imposing monotonic loads equivalent to damage levels induced by seismic loadings. A full-scale test on a reinforced concrete frame of dimensions 3 m x 3 m x 3 m has been recently performed by Kamath and co-workers [7] to

investigate its fire performance after a seismic event. A large-scale test was carried out at the University of San Diego [8], [9] to study the post-earthquake performance of a 5-story reinforced concrete building.

Lightweight framing systems are commonly used in single-story buildings and for internal partitions in multistory buildings. However, they are also used for the structural systems in multi-story buildings, combined with other structural typologies. As an example, the lightweight structural systems using cold-formed steel currently represent about 20 % of the nonresidential construction market in the United States and this is mainly for their cost advantages and increased construction speed. The fire performance of the lightweight structures is an important consideration for tall buildings because as buildings get taller, evacuation time increases and extinguishing the fire becomes more challenging. Nevertheless, there is limited knowledge about the behavior of cold-formed steel systems under combined hazards, in particular, earthquake, and fire [10]. Gypsum plasterboard (GPB)-based wall assemblies are widely used in constructions and they usually consist of GPB, insulation and steel studs. Cost advantage, increased construction speed and proper fire resistance behavior are the main reasons which make this system popular. The probability of GPB to exhibit some damage during the earthquake is high and this can have repercussions in the case of FFE. GPB exhibits good fire resistance because it is composed of around 20% of chemically bound water and 3% of free water and, therefore, the heat transfer through the material is delayed when the GPB undergoes endothermic processes to release the water. The fire behavior of the walls is highly dependent on GPBs thermo-mechanical properties. Numerous studies (e.g., [11], [12]) focused on the thermal behavior of the GPBs because it is often used as passive fire resistance elements. Only a few studies (e.g., [13]-[15]) focused on the mechanical properties of GPBs at elevated temperatures. The mechanical properties of the GPBs are temperature dependent, reaching low values after complete calcination. Since there is no proposed procedure to establish the mechanical properties of GPBs, three-point bending or four-point bending tests were used to retrieve them. Only a limited number of numerical simulations of GPB walls are available in the literature (e.g. [13], [16]) due to the complexity of the material properties.

In order to enable FFE experimentation of GPB-based walls, a hybrid fire testing (HFT) platform is being developed at the Danish Institute of Fire and Security Technology (DBI). HFT [17], [18] can be viewed as a conventional finite element analysis that is extended by additionally involving experimentally investigated members. The analyzed structure is divided into a numerical substructure (NS) and a physical substructure (PS) that are coupled and continuously exchange data during the analysis. If members represent parts of the structure with unknown or partially unknown thermo-mechanical behavior, then it is recommended to physically test them. The parts of the structure with a well-known thermo-mechanical behavior are numerically modeled. The HFT procedure will make sure that the test and the numerical analysis are connected in such a way that the response of the prototype structure is reproduced. This paper provides an overview of the current state of developments including a preliminary numerical verification of the setup.

2 The hybrid fire testing framework

2.1 Description of the setup

The HFT setup was conceived to test GPB-based wall assemblies which can be exposed to elevated temperatures on surfaces of an approximate size of 500 x 500 mm. Fig. 1 provides a schematic overview of the HFT setup in the form of a block diagram. The hybrid model of the prototype structure consists of a single-degree-of-freedom (DoF) system, which couples a single-DoF PS and a single-DoF NS both assimilated to truss elements. The PS consists of a gypsum plasterboard, which is installed on a loading frame fitting an electric furnace. The hybrid model communicates to the experimental setup through a middleware based on an INDEL real-time computer equipped with analog DAQ boards. Proportional-Integral (PI) controllers are used to adjust both axial elongation and temperature of the tested specimen, that is, the PS. The time history response of the hybrid model is computed in a Python [19] simulation environment, which communicates to the INDEL RT system with a dedicated API.

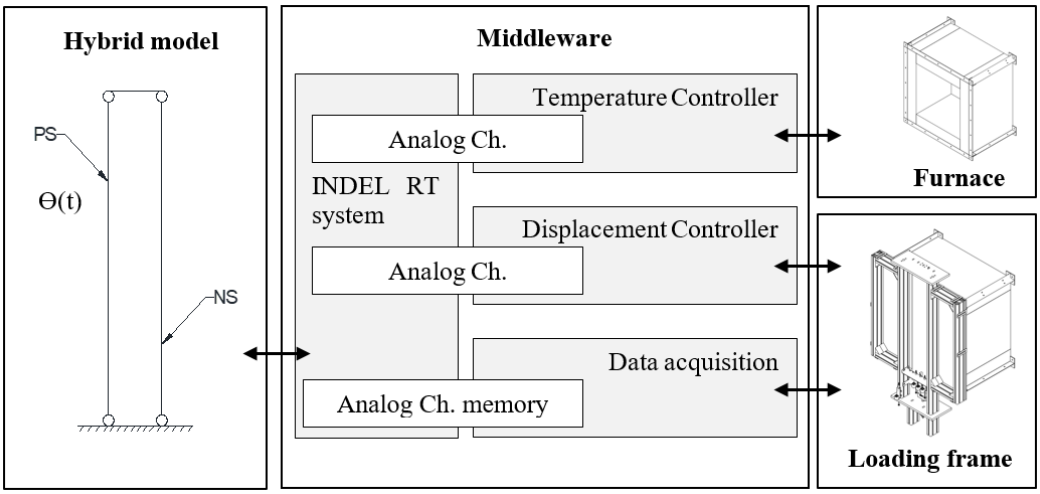

Fig. 1 – Schematic overview of the HFT setup.

Fig. 2 presents an overview of the experimental setup used to apply or measure temperatures, displacements, and force on the PS (1).

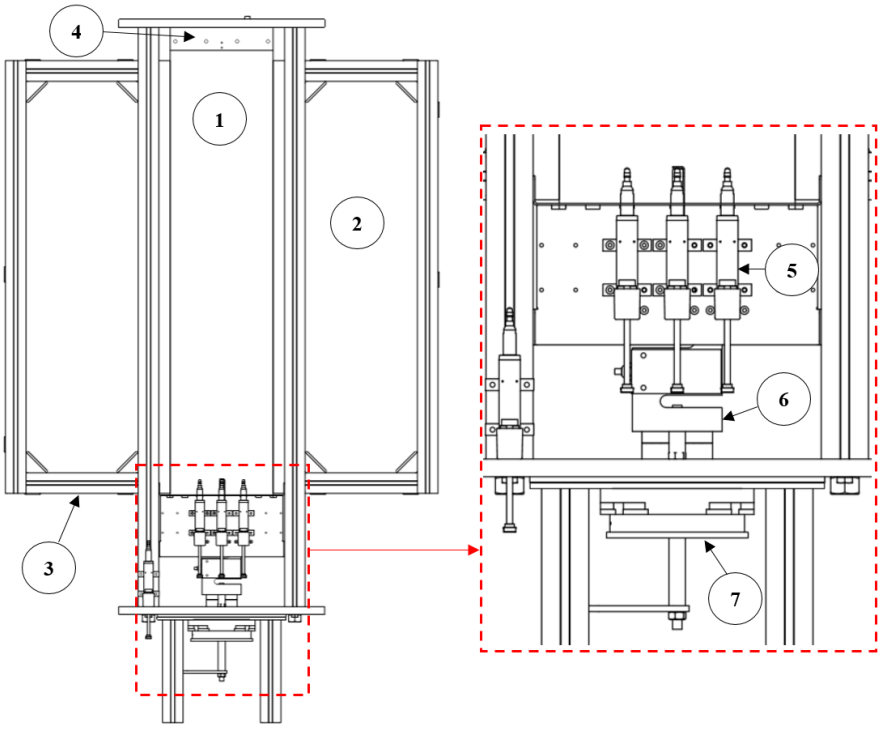

Fig. 2 – HFT test rig at DBI. (1): PS, (2): Calcium silicate board, (3): Aluminum frame, (4): PS fixation, (5): Linear displacement transducer, (6): S-load cell, (7): Rotary motor.

The designed test rig will be attached to the DBI mobile furnace, allowing exposure on one side of the PS. The mobile furnace test apparatus is developed by DBI and designed to perform fire tests on small-scale specimens, having the exposure dimensions of 500 × 500 mm. The DBI furnace can deliver a maximum of approximately 20 kW by electrical heating and is capable of running multiple fire curves. The furnace temperature is controlled using three shielded 3 mm type K thermocouples positioned close to the specimen at various positions inside the furnace. No correction for radiation on the bead was performed. The skeleton of the test rig is symmetric and is made out of the aluminum members (3). The PS is screwed to the fixations (4)

at both ends. The bottom fixation is connected to the rotary motor (7) which will control the axial displacement of the PS. In between the rotary motor and the bottom fixation, the PT-Global model PT4000-500 kg S-load cell (6) measures the axial reaction force of the PS. The axial displacement of the PS is measured using Megatron SPR 18-50 linear displacement transducers (5). Three displacement transducers are used to measure the displacement of the board at predefined locations while one displacement transducer is used to measure the thermal elongation of the aluminum profile. In order to keep a low temperature of the aluminum members, calcium silicate boards (2) are fixed on the test rig and along with the PS will be the only elements directly exposed to heat. The measurement instruments are placed at the bottom of the test rig, away from the hot zone to reduce the effect of temperature on the measurements. The temperature of the unexposed side of PS is measured using 4 type K thermocouples model FT-50511102-0200.12.GG.D from GUENTHER Polska, three of them are equally distributed in the heated zone, while one of them is placed on the unheated zone. The length of the PS is cut to 950 mm, where only 500 mm is exposed to elevated temperatures. The GPB is cut longer than the heated zone dimension so that the fixations are outside of the heated zone.

The measurement system for HFT was characterized prior the start of the testing program and is summarized in Table 1.

Table 1 – Sensors used in the experiment.

Sensor Description	Manufacturer	Model	Full-Scale Value
Specimen Thermocouples	GUENTHER Polska	FT-50511102-0200.12.GG.D	1250 °C
S-Beam Load Cell	PT-Global	PT4000-500kg	500 kg
Potentiometric Linear Transducer	Megatron	SPR 18-50	50 mm

2.2 Time integration algorithm

The coupled equations of motion of the hybrid system are solved with a partitioned time integration approach. An interface force represented by a Lagrange multiplier imposes velocity compatibility between single-DoF PS and NS. The coupled solution is computed with a two-stage approach where interface forces are computed by solving a linearized dual problem. The coupled equation of motion of the single-DoF hybrid systems read,

$$m^P \ddot{x}_k^P + c^P \dot{x}_k^P + r^P(x_k^P, \dot{x}_k^P, \theta_k^P) = l^P \Lambda_k + f^P(t_k) \quad (1)$$

$$m^N \ddot{x}_k^N + c^N \dot{x}_k^N + r^N(x_k^N, \dot{x}_k^N, \theta_k^N) = l^N \Lambda_k + f^N(t_k) \quad (2)$$

$$l^P \dot{x}_k^P + l^N \dot{x}_k^N = 0 \quad (3)$$

Where x^*, $\dot{x}^*$ and $\ddot{x}^*$ represent displacement, velocity and acceleration while θ^* is the temperature; m^* and c^* are mass and damping matrices, respectively, whereas r^* is the restoring force. l^* is a Boolean variable that determines the orientation of the interface force Λ. External time-varying load is represented by $f^*(t)$. Superscripts P and N stand for PS and NS, respectively. For the earthquake simulation, mass and damping matrices of the system are computed from structural properties whereas the external loading is defined as,

$$f^*(t) = -m^* a_g(t) \quad (4)$$

Where $a_g(t)$ is a seismic acceleration history. On the other hand, the structural response to fire loading is static. Therefore, fictitious mass and damping matrices $\hat{m}^*$ and $\hat{c}^*$, respectively, replace mass and damping matrices in Eq. (1) & (2). Values are computed according to the dynamic relaxation method proposed by Underwood [20] as,

$$\hat{m}^* = \frac{(1.1\Delta t)^2 |k^*|}{4} \quad (5)$$

$$\hat{c}^* = 2\omega\hat{m}^* \tag{6}$$

Where Δt is the time step, k^* is the stiffness and ω is the eigenfrequency of the coupled system, which reads,

$$\omega = \sqrt{\frac{k^P + k^N}{\hat{m}^P + \hat{m}^N}} \tag{7}$$

Accordingly, the solution of Eq. (1) & (2) mimics the response of a static system. In principle, a smaller time step is used for the –dynamic- earthquake analysis (e.g., 1 ms) and a larger for the –static- fire analysis (e.g., 1 s). A detailed description of the proposed method is reported in [21].

2.3 Quantification of experimental errors

In order to support a numerical verification of the HFT setup that includes all sources of experimental errors, Type A and/or Type B uncertainties, combined standard uncertainties, and total expanded uncertainties were estimated for each sensor and actuation device, as defined in Taylor and Kuyatt [22]. Type A uncertainty is evaluated using statistical methods and Type B uncertainty is estimated by other means such as the information available in the manufacturer's specifications, from past-experience, or engineering judgment. The combined standard uncertainty is estimated by combining the individual uncertainties using "root-sum-of-squares". The expanded uncertainty is then computed by multiplying the combined uncertainty by a coverage factor of 2 corresponding to an approximately 95 % confidence interval. All uncertainties are assumed to be symmetric (±). Table 2 summarizes the estimated uncertainties of the measurements.

Table 2 – Uncertainty in the experimental data

Measurement/Component	Estimation Method of Uncertainty	Component Standard Uncertainty	Combined Standard Uncertainty	Total expanded Uncertainty (k=2)
Specimen Temperature				
Calibration	Type B	±0.55 %	±5.73 %	±11.47 %
Installation	Type B	±5.60 %		
Random	Type A	±1.10 %		
Load				
Zero	Type B	±0.33 %	±1.17 %	±2.34 %
Linearity	Type B	±0.02 %		
Installation	Type B	±0.38 %		
Random	Type A	±1.00 %		
Repeatability	Type A	±0.34 %		
Displacement				
Linearity	Type B	±0.10 %	±0.40 %	±0.80 %
Installation	Type B	±0.38 %		
Random	Type A	±0.06 %		
Repeatability	Type A	±0.07 %		

The following definitions are used:

- *Calibration, zero, linearity*: Uncertainties from known sources of error and derived from instrument specifications (Type B).
- *Installation*: Uncertainty due to installation and estimated based on engineering judgment (Type B).
- *Random*: Uncertainty due to random, unpredictable variations in the measurement process during a typical steady-state period and derived using the standard deviation of the residuals from the mean value of the measurements (Type A).

- *Repeatability*: Uncertainty when measuring the same point multiple times during a typical steady-state period (Type A).

The installation effect on temperature measurements was evaluated considering the following parameters: welding technique of the thermocouples; weight, thickness and density of the pad; and type of the glue, respectively. The installation effect on the load and displacement measurements was evaluated considering an installation error of 5 degrees.

3 A numerical verification of the framework

3.1 GPB-based wall assembly

The case study illustrated in Fig. 3, which corresponds to a GPB-based wall assembly, was used as a reference prototype structure to develop the presented HFT setup. Accordingly, it was used to support a numerical verification that accounts for the main sources of experimental errors.

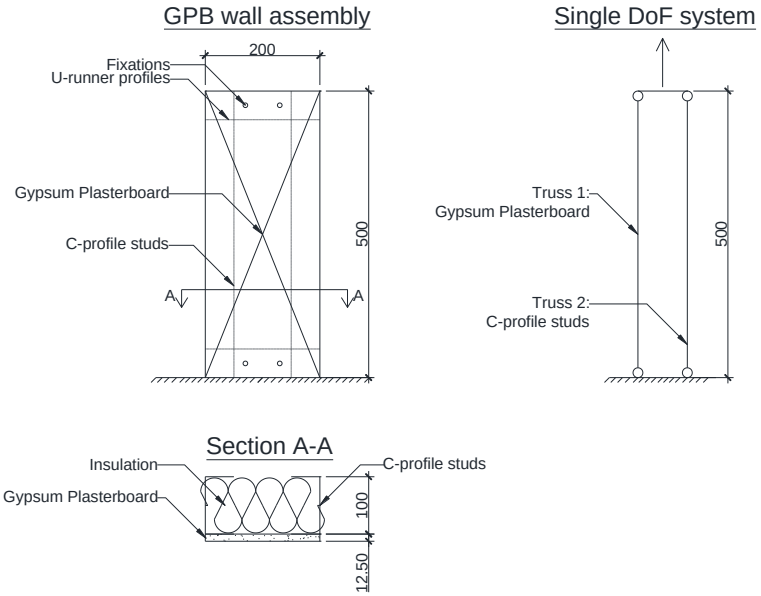

Fig. 3 – GPB-based wall assembly and the corresponding hybrid model.

The prototype structure of Fig. 3 was reduced to a single-DoF system composed of two trusses defined by their stiffness, free to expand in the vertical direction. The two trusses represent a standard GPB and the C.100.50.12 steel studs, respectively. The characteristics of the steel stud profile are detailed in [23] while Eurocode 3 [24] steel material properties at elevated temperatures, e.g., the elastic modulus and the thermal elongation, are considered. The mechanical properties of the GPBs at elevated temperatures, e.g., the elastic modulus and the stress at failure, are derived from a series of tensile tests which were performed on samples of 12.5 × 200 × 950 mm (thickness × width × length) under fire conditions to compare the behavior at different elevated temperatures. First, the specimen was heated for an hour to ensure the steady-state temperature distribution within the cross-section. Then tensile loading was ramped up until failure. From the test results, material stress-strain curves at different temperatures are derived with the purpose to be used later in the numerical simulations. In this regard, Fig. 4 illustrates the stress-strain curves developed for standard plasterboard. It can be seen that over 500 °C the material degrades significantly. The thermal expansion behavior of the GPBs was assumed as in [13]. Gypsum thermally expands in the very first stage of the fire followed by contraction whereas Young modulus constantly decreases with the increase of temperature.

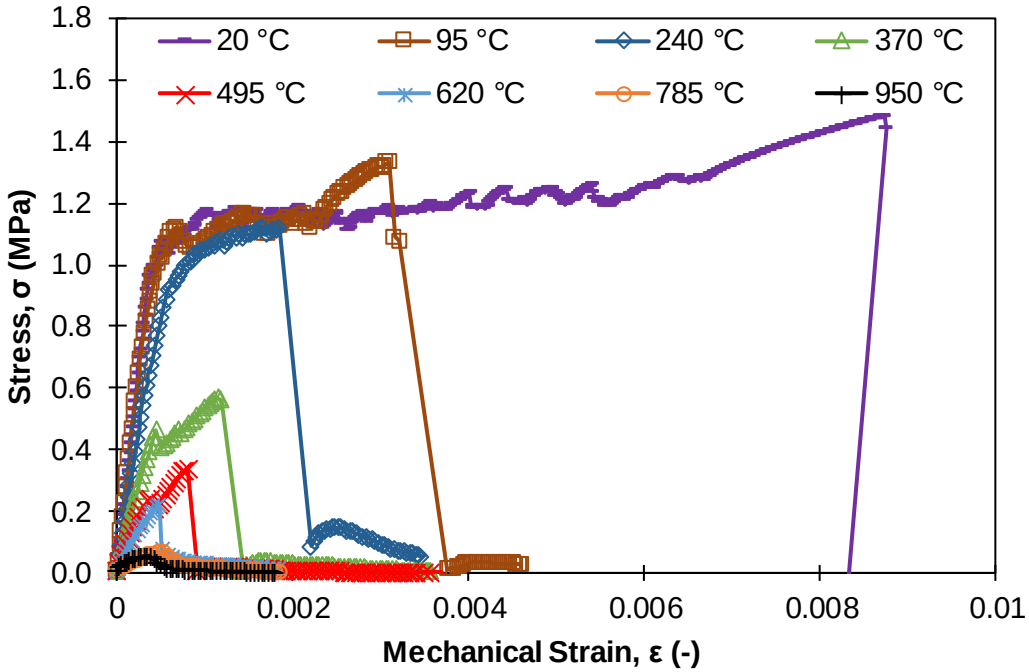

Fig. 4 – Derived stress-strain curve for gypsum at elevated temperatures

3.2 Virtual hybrid testing campaign

A numerical HFT simulation of the GPBs-based walls subjected to FFE was peformed in MATLAB [25], considering restoring force noise, displacement control error and temperature control error as sources of experimental errors. A variant of the bilinear hysteretic spring proposed by Mostaghel [26] was used to simulate the thermoplastic restoring force of both PS and NS. The main equations of hysteretic spring read,

$$\dot{\sigma} = E_P \dot{\epsilon}_{mec} + (E_E - E_P)\dot{u} \tag{8}$$

$$\dot{u} = \left[\bar{N}(\dot{\epsilon}_{mec})\bar{M}\left(u - \epsilon_y\right) + M(\dot{\epsilon}_{mec})N\left(u + \epsilon_y\right)\right]\dot{\epsilon}_{mec} \tag{9}$$

where r is the restoring force, u is an internal memory variable and $\epsilon_{mec} = \epsilon - \epsilon_{ter}$ is the mechanical strain of the specimen whereas the thermal strain is computed as $\epsilon_{ter} = \alpha\theta$, where α is the coefficient of thermal expansión. E_E and E_P are elastic and hardening modulus of the single-DoF spring whereas ϵ_y is the yielding strain. The remaining functions $N, M, \bar{N}$ and $\bar{M}$ are defined as follows,

$$N(v) = 0.5\left(1 + sign(v)\right)\left(1 + \left(1 - sign(v)\right)\right) \tag{10}$$

$$M(v) = 1 - N(v) \tag{11}$$

$$\bar{N}(v) = M(-v) \tag{12}$$

$$\bar{M}(v) = N(-v) \tag{13}$$

Where v is a dummy variable in this case. Table 3 summarizes the parameters of both PS and NS. For the sake of simplicity, the temperature dependence of material parameters has been neglected in the simulation of the HFT except for the thermal expansion coefficient.

Table 3 – Parameters of the hybrid model.

Description	Symbol	Value	Symbol	Value
Elastic modulus [MPa]	E_E^N	210000	E_E^P	2444
Hardening modulus [MPa]	E_P^N	2100	E_P^P	27
Yielding stress [MPa]	f_y^N	450	f_y^P	1.1
Cross-section area [mm^2]	A^N	532	A^P	2500
Length [mm]	L^N	500	L^P	500
Mass [kg]	m^N	2.83	m^P	0.97

Prior to the fire exposure, the dynamic response of the hybrid model was evaluated considering an acceleration record of the Loma Prieta [27] earthquake as loading excitation. Next, the system was subjected to a temperature ramp from the ambient temperature up to 150 °C to simulate FFE. In this latter case, the static response of the hybrid model was computed with the dynamic relaxation approach reported in Section 2.2. The effect of the seismic load was to induce a permanent deformation of the GPB-based wall before the initiation of fire. Fig. 5 shows the evolution of displacement and force at the interface of the single-DoF system during FFE.

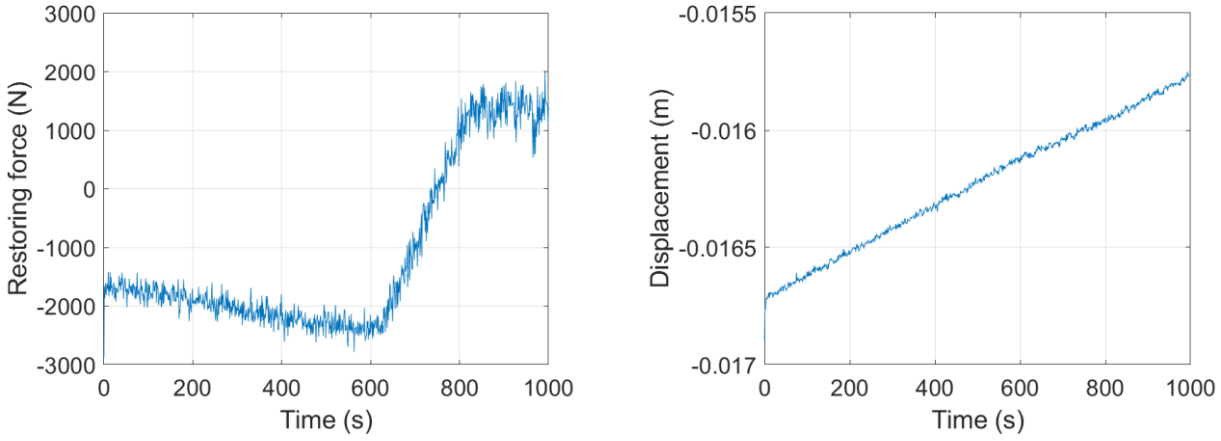

a) b)

Fig. 5 – Time history response of the PS during FFE: a) restoring force; b) total displacement.

As can be appreciated from Fig. 5, the numerical simulation highlighted the satisfying performance of the proposed HFT framework in the presence of noise. Moreover, restoring force, displacement and temperature ranges are compatible with the experimental setup.

4 Conclusions and future work

The potential of HFT for enabling a better understanding of the global structural response to fire following earthquakes is discussed in this paper. The architecture that allows performing the static or dynamic hybrid fire tests developed at the DBI is introduced. The studied benchmark problem is a GPB-based wall system represented in the first stage of the project as a single-DoF system. Before the validation of the HFT test rig at DBI, the errors of the experimental setup, as the properties of the PS at elevated temperatures were investigated. Numerical simulation of the system was performed in MATLAB and it will be followed by the experimental validation.

5 References

[1] Scawthorn C, Eidinger JM, Schiff AJ (2005): Fire following earthquake. Technical Council on Lifeline Earthquake Engineering Monograph, No. 26. American Society of Civil Engineers

[2] Mousavi S, Bagchi A, Kodur VKR (2008): Review of post-earthquake fire hazard to building structures, *Canadian Journal of Civil Engineering*, 35:689-698.

[3] EQE, The January 17, (1995): Kobe earthquake. *An EQE Summary Report*, EQE International.

[4] Taylor J (2003): Post earthquake fire in tall buildings and the New Zealand code. Research project report, University of Canterbury, Christchurch, New Zealand.

[5] Pucinotti R, Bursi OS, Demonceau JF (2011): Post-earthquake fire and seismic performance of welded steel–concrete composite beam-to-column joints, *Journal of Constructional Steel Research*, 67:1358–1375.

[6] Pucinotti R, Bursi OS, Franssen JM, Lennon T (2011): Seismic-induced fire resistance of composite welded beam-to-column joints with concrete-filled tubes, Fire Safety Journal, 46:335–347.

[7] Kamath P, Sharma UK, Kumar V, Bhargava P, Usmani A, Singh B, Singh Y, Torero J, Gillie M, Pankaj P (2015): Full-scale fire test on an earthquake-damaged reinforced concrete frame, *Fire Safety Journal*, 73:1–19.

[8] Meacham BJ (2016): Post-Earthquake Fire Performance of Buildings: Summary of a Large-Scale Experiment and Conceptual Framework for Integrated Performance-Based Seismic and Fire Design, Fire Technology, 52(4):1133–1157.

[9] Pantoli E, Chen M, Wang X, Astroza R, Ebrahimian H, Hutchinson T, … Faghihi M (2016): Full-Scale Structural and Nonstructural Building System Performance during Earthquakes: Part II – NCS Damage States, *Earthquake Spectra*, 32(2): 771–794.

[10] Hoehler MS, Andres VB, Bundy M (2019): Influence of Fire on the Lateral Resistance of Cold-Formed Steel Shear Walls. Phase 2: Oriented Strand Board, Strap Braced, and Gypsum-Sheet Steel Composite. NIST TN – 2038.

[11] Thomas G (2002): Thermal Properties of Gypsum Plasterboard at High Temperatures. *Fire Mater*. 26, 37 45.

[12] Park S, Manzello S, Bentz D. P & Mizukami T (2009): Determining Thermal Properties of Gypsum Board at Elevated Temperatures. *Fire Mater*. doi:10.1002/fam.

[13] Rahmanian I (2011): Thermal and Mechanical Properties of Gypsum Boards and their Influences on Fire Resistance of Gypsum Board Based Systems. *PhD thesis*, (University of Manchester, 2011).

[14] Cramer SM, White RH, Sriprutkiat G & Friday OM (2003): Mechanical Properties of Gypsum Board at Elevated Temperatures. *Fire and materials 2003 : 8th International Conference*, San Francisco, CA, USA. London : Interscience Communications Limited, c2003: pages 33-42.

[15] Andres B, van Hees P (2016): Mechanical Properties of Gypsum Plasterboard Exposed to Standard Fires, INTERFLAM 2016, *14th International Conference and Exhibition on Fire Science and Engineering*.

[16] Tran H (2012): Etude numérique et expérimentale du comportement au feu des éléments séparatifs en plaques de plâtre à ossature acier. *PhD thesis*, L'ecole Normale Superieure de Cachan, France.

[17] Korzen M, Magonette G, Buchet Ph (1999): Mechanical loading of columns in fire tests by means of the substructuring method. *Zeitschrift für Angewandte Mathematik und Mechanik*, 79: S617-S618.

[18] Sauca A, Gernay T, Robert F, Tondini N, Franssen J-M (2018): Hybrid fire testing: discussion on stability and implementation of a new method in a virtual environment. *J. Struct. Fire Eng.*, 9 (4) (2018), pp. 319-341.

[19] Python Software Foundation. Python Language Reference, version 2.7. Available at http://www.python.org (Accessed 14 February 2020).

[20] Underwood PG (1983): Dynamic relaxation techniques: a review. *Computational Methods for Transient Analysis*, Amsterdam, North-Holland.

[21] Abbiati G, Covi P, Tondini N, Bursi OB, Stojadinovic B (2020): A Real-Time Hybrid Fire Simulation Method Based on Dynamic Relaxation and Partitioned Time Integration, Submitted to *ASCE Journal of Engineering Mechanics*.

[22] Taylor BN, Kuyatt CE (1994): Guidelines for Evaluating and Expressing the Uncertainty of NIST Measurement Results, NIST (1994), *Technical Note 1297*.

[23] Drywall Steel Sections Ltd (DSSL). Light Steel Framing (LSF) Product Information. https://www.drywallsteelsections.co.uk/assets/files/attached/196/Light-Steel-Framing.pdf (Accessed 21 January 2020).

[24] EN 1993-1-2 (2005): Eurocode 3: Design of steel structures - Part 1-2: General rules - Structural fire design, [Authority: The European Union per Regulation 305/2011, Directive 98/34/EC, Directive 2004/18/EC].

[25] MATLAB 7.10.0, *Natick, Massachusetts*, The MathWorks Inc. (2016).

[26] Mostaghel N (1999): Analytical Description of Pinching, Degrading Hysteretic Systems. *Journal of Engineering Mechanics*, vol. 125, no. 2, pp. 216-224, 1999.

[27] PEER Pacific Earthquake Engineering Research (PEER) Center (2016): *Ground Motion Database*, May 24, 2016.

